Gas phase formation of c-SiC$_3$ molecules in the circumstellar envelope of carbon stars

Tao Yang[a,b,1,2], Luke Bertels[c,1], Beni B. Dangi[b,3], Xiaohu Li[d,e], Martin Head-Gordon[c,2], and Ralf I. Kaiser[b,2]

[a]State Key Laboratory of Precision Spectroscopy, East China Normal University, Shanghai 200062, P. R. China; [b]Department of Chemistry, University of Hawai'i at Mānoa, Honolulu, HI 96822; [c]Department of Chemistry, University of California, Berkeley, CA 94720; [d]Xinjiang Astronomical Observatory, Chinese Academy of Sciences, Urumqi, Xinjiang 830011, P. R. China; and [e]National Astronomical Observatories, Chinese Academy of Sciences, Beijing 100012, P. R. China

Complex organosilicon molecules are ubiquitous in the circumstellar envelope of the asymptotic giant branch (AGB) star IRC+10216, but their formation mechanisms have remained largely elusive until now. These processes are of fundamental importance in initiating a chain of chemical reactions leading eventually to the formation of organosilicon molecules—among them key precursors to silicon carbide grains—in the circumstellar shell contributing critically to the galactic carbon and silicon budgets with up to 80% of the ejected materials infused into the interstellar medium. Here we demonstrate via a combined experimental, computational, and modeling study that distinct chemistries in the inner and outer envelope of a carbon star can lead to the synthesis of circumstellar silicon tricarbide (c-SiC$_3$) as observed in the circumstellar envelope of IRC+10216. Bimolecular reactions of electronically excited silicon atoms (Si(^{1}D)) with allene (H$_2$CCCH$_2$) and methylacetylene (CH$_3$CCH) initiate the formation of SiC$_3$H$_2$ molecules in the inner envelope. Driven by the stellar wind to the outer envelope, subsequent photodissociation of the SiC$_3$H$_2$ parent operates the synthesis of the c-SiC$_3$ daughter species via dehydrogenation. The facile route to silicon tricarbide via a single neutral–neutral reaction to a hydrogenated parent molecule followed by photochemical processing of this transient to a bare silicon–carbon molecule presents evidence for a shift in currently accepted views of the circumstellar organosilicon chemistry, and provides an explanation for the previously elusive origin of circumstellar organosilicon molecules that can be synthesized in carbon-rich, circumstellar environments.

reaction dynamics | circumstellar envelopes | organosilicon molecules | astrochemistry

For the last decades, the carbon-rich asymptotic giant branch (AGB) star IRC+10216 (CW Leo) has been widely recognized as a rich, natural laboratory for advancing our fundamental understanding of the chemical evolution of the carbon-rich circumstellar envelopes through astronomical observations combined with astrochemical modeling exploiting complex gas phase reaction networks involving ion–molecule (1–6) and neutral–neutral reactions (4, 5, 7–11). However, with about 80 molecules detected in circumstellar environments (12)—primarily hydrogen-deficient carbon chains and molecules with exotic chemical bonding containing metals and silicon—these models have, as yet, failed to account for the synthesis of ubiquitous silicon carbide molecules and forecasting their molecular fractional abundances, such as cyclic silicon dicarbide (c-SiC$_2$) (13), bicyclic silicon tricarbide (c-SiC$_3$) (14), and linear silicon tetracarbide (SiC$_4$) (15), which diverge by up to two orders of magnitudes compared with astronomical observations (16, 17). Hence, although circumstellar molecules—precursors to silicon carbide grains among them—contribute critically to the galactic carbon and silicon budgets with up to 80% of the ejected material infused into the interstellar medium (18, 19), the formation routes of organosilicon molecules in circumstellar envelopes and the fundamental processes involved in coupling the carbon and silicon chemistries are largely unknown to date (17, 20, 21).

Modern astrochemical models propose that the very first silicon–carbon bonds are formed in the inner envelope of the carbon star, which is undergoing mass loss at the rates of several 10^{-5} solar masses per year (22, 23). Pulsations from the central star may initiate shocks, which (photo)fragment the circumstellar materials (24, 25). These nonequilibrium conditions cause temperatures of 3,500 K or above (19) and lead to highly reactive metastable fragments such as electronically excited silicon atoms, which can attack hydrocarbon molecules to initiate the formation of silicon–carbon bonds (24, 26). The newly synthesized molecules are proposed to be driven by the stellar wind to the outer envelope, where they are photolyzed by the interstellar UV field (24). Considering the strength of silicon–carbon double (450–550 kJ mol^{-1}) versus carbon–hydrogen single (about 400 kJ mol^{-1}) bonds, the photochemistry is expected to preferentially cleave carbon–hydrogen bonds, eventually synthesizing bare silicon–carbon molecules. However, the validity of these processes has not been confirmed, although these pathways are fundamental to an intimate understanding of the evolution of circumstellar envelopes at the molecular level, eventually constraining the pathways to bare silicon–carbon molecules in our galaxy.

Significance

Since the detection of methylidyne (CH) in deep space over 80 y ago, about 200 molecules and molecular ions from molecular hydrogen to fullerenes have been observed in interstellar and circumstellar environments, but the synthesis of organosilicon molecules has remained largely elusive. Exploiting silicon tricarbide (c-SiC$_3$) as a benchmark, we provide evidence from laboratory experiments, electronic structure calculations, and astrochemical modeling that organosilicon species can be synthesized via distinct chemistries in the inner and outer envelope of carbon stars like IRC+10216 via bimolecular reactions followed by photochemical dehydrogenation to bare silicon carbon molecules. These mechanisms are of fundamental significance to facilitate an understanding how carbon and silicon chemistries can be coupled to synthesize organosilicon molecules in the universe.

To fill this gap, we present a combined crossed molecular beam, high-level ab initio, and astrochemical modeling investigation on the formation of (hydrogenated) circumstellar silicon tricarbide (c-SiC$_3$) via distinct chemistries in the inner and outer envelope of the carbon star IRC +10216. The reactions of electronically excited silicon atoms (Si(^{1}D)) with allene (H$_2$CCCH$_2$) and methylacetylene (CH$_3$CCH) (reaction **I**) were explored under single collision conditions, revealing first the formation of distinct SiC$_3$H$_2$ isomers in the inner envelope of IRC+10216. Ejected by the stellar wind to the outer envelope, photochemical processing of these SiC$_3$H$_2$ parent molecules leads to the synthesis of the bicyclic silicon tricarbide daughter species as observed in the envelope of IRC+10216 via dehydrogenation (reaction **II**).

$$Si(^1D) + C_3H_4 \rightarrow SiC_3H_2 + H_2 \qquad \textbf{[I]}$$

$$SiC_3H_2 + h\nu \rightarrow c\text{-}SiC_3 + H_2 \qquad \textbf{[II]}$$
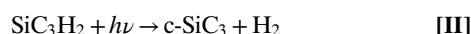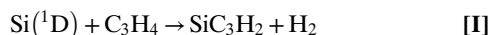
Results

Crossed Molecular Beam Studies—Laboratory Frame. The gas phase reactions of electronically excited silicon atoms (Si(^{1}D)) with allene (H$_2$CCCH$_2$) and methylacetylene (CH$_3$CCH) were explored experimentally under single collision conditions in a crossed molecular beam machine by intersecting supersonic beams of electronically excited silicon atoms with the hydrocarbon beams perpendicularly at collision energies of 30 ± 2 kJ mol^{-1} (*Materials and Methods*). The primary beam, generated via photolysis of 0.5% disilane seeded in helium, contains ground and excited state silicon atoms (Si(^{3}P)/Si(^{1}D)) along with the silylidyne radical (SiH(X^{2}Π)). The reaction dynamics of the silylidyne radical with allene and methylacetylene have been explored previously (27, 28), while ground state silicon atoms do not react with allene or methylacetylene (*SI Appendix*). Therefore, the present study allows us to discriminate scattering signal

obtained via the reaction of electronically excited silicon atoms from that obtained via the reaction of the silylidyne radical with allene and methylacetylene, respectively. These neutral reaction products were ionized via electron impact at 80 eV within a triply differentially pumped quadrupole mass-spectrometric detector, and then mass and velocity analyzed to record time-of-flight (TOF) spectra of the ionized products (29). First, in both systems, reactive scattering signal with allene and methylacetylene was observed at mass-to-charge ratio (m/z) of 68 (SiC$_3$H$_4^+$), 67 (SiC$_3$H$_3^+$), and 66 (SiC$_3$H$_2^+$). Signal at m/z of 68 (SiC$_3$H$_4^+$) was found to originate from the reaction of the silylidyne radical (SiH(X^{2}Π)) with allene and methylacetylene leading to the formation of 2-methyl-1-silacycloprop-2-enylidene (c-SiC$_3$H$_4$) plus atomic hydrogen (27, 28). Second, in both reactions, the TOF spectra at m/z of 68 (SiC$_3$H$_4^+$) and 67 (SiC$_3$H$_3^+$) were indistinguishable after scaling, revealing that signal at m/z of 67 originates from the dissociative electron impact ionization of the 2-methyl-1-silacycloprop-2-enylidene parent molecules in the electron impact ionizer. Third, TOF spectra taken at m/z of 66 (SiC$_3$H$_2^+$) for both systems are distinct compared with the TOFs taken at m/z of 68 (SiC$_3$H$_4^+$) and 67 (SiC$_3$H$_3^+$). Therefore, the signal at m/z of 66 does not solely arise from dissociative ionization of the SiC$_3$H$_4$ parent products formed in the reaction of the silylidyne radical with allene and methylacetylene, but also from a molecular hydrogen loss channel in the reaction of the excited silicon with allene and methylacetylene leading to SiC$_3$H$_2$ isomer(s) (reaction **I**), provided that the ground silicon does not react with these two C$_3$H$_4$ isomers under our experimental conditions. Fig. 1 depicts the laboratory angular distributions and selected TOF spectra recorded at m/z of 66 (SiC$_3$H$_2^+$), which were found to be fitted in two separated reaction channels. The first channel arises from the dissociative ionization of the SiC$_3$H$_4$ product from the silylidyne radical reaction with allene and methylacetylene, whereas the second channel originates from reactive scattering within the Si(^{1}D)–C$_3$H$_4$ systems leading to

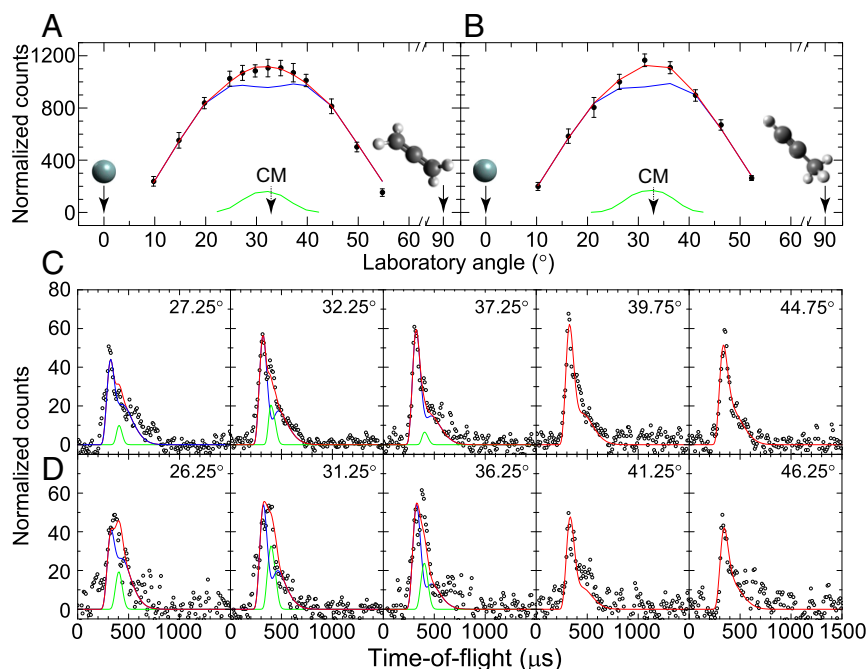**Fig. 1.** Laboratory angular distributions and selected TOF spectra. Laboratory angular distributions of the products recorded at m/z of 66 (SiC$_3$H$_2^+$) for the reactions of Si(^{1}D) (blue) and SiH(X^{2}Π) (green) with allene (*A*) or methylacetylene (*B*), respectively. The solid circles represent the experimental data, CM designates the center-of-mass angle, the error bars represent the 1 σ SD, and red solid lines represent the overall fit. Selected TOF spectra in *C* and *D* represent the reactions of Si(^{1}D) (blue) and (SiH(X^{2}Π)) (green) with allene (*C*) or methylacetylene (*D*) with the overall fit defined by the red lines, while the open circles depict the experimental data points.

SiC$_3$H$_2$ product(s) via molecular hydrogen losses (reaction **I**). Quantitatively, the contributions of the SiH–C$_3$H$_4$ system presents a minor channel accounting for about 10% of the ion signal at m/z of 66. As revealed in Fig. 1, the laboratory angular distributions spread over 45° and are nearly forward–backward symmetric around the center-of-mass (CM) angle of 33° for the Si(^{1}D) reactions with both C$_3$H$_4$ isomers. These data suggest that both Si(^{1}D) reactions with allene and methylacetylene proceed by indirect reaction dynamics involving the formation of SiC$_3$H$_4$ complex(es).

Having established that in the reactions of excited state atomic silicon with allene and methylacetylene, the molecular hydrogen loss leads to the formation of SiC$_3$H$_2$ isomer(s) (reaction **I**), we are attempting now to elucidate the position of the molecular hydrogen loss. This can be conducted for the methylacetylene reactant since the methyl and acetylenic hydrogen atoms are chemically nonequivalent, and its partially deuterated D3-methylacetylene reactant is commercially available. Reaction with Si(^{1}D) can proceed via HD loss to the formation of SiC$_3$D$_2$ (68 amu) (reaction **III**), whereas molecular deuterium (D$_2$) loss should yield signal at m/z of 67 (SiC$_3$DH) (reaction **IV**). Note that products formed via the HD loss (SiC$_3$D$_2$) cannot undergo dissociative electron impact ionization to signal at m/z of 67. Therefore, ions detected at m/z of 68 and 67 originate—with the exception of 3.3% ^{13}C and 5.1% ^{29}Si substituted products—from SiC$_3$D$_2^+$ and SiC$_3$DH$^+$, respectively. Fig. 2 shows the TOF data collected for the HD and D$_2$ losses at m/z of 68 (SiC$_3$D$_2^+$) and 67 (SiC$_3$DH$^+$) for the reaction of Si(^{1}D) with D3-methylacetylene. Due to the high cost of D3-methylacetyene, data were collected only at the respective CM angle. As evident from Fig. 2, we detected signal at m/z of 68 (SiC$_3$D$_2^+$) and 67 (SiC$_3$DH$^+$) related to the HD and D$_2$ loss with branching ratios of $60 \pm 15\%$ and $40 \pm 15\%$, respectively. Overall, we conclude that in the reaction of electronically excited silicon atoms with D3-methylacetylene, both the hydrogen deuteride and molecular deuterium loss channels are open leading to distinct isomers.

$$\text{Si}\left(^1\text{D}\right) + \text{CD}_3\text{CCH} \rightarrow \text{SiC}_3\text{D}_2 + \text{HD} \qquad \textbf{[III]}$$

$$\text{Si}\left(^1\text{D}\right) + \text{CD}_3\text{CCH} \rightarrow \text{SiC}_3\text{DH} + \text{D}_2 \qquad \textbf{[IV]}$$

Crossed Molecular Beam Studies—Center-of-Mass Frame. The interpretation of the raw data provided conclusive evidence that in the reaction of excited silicon atoms with allene and methylacetylene, an organosilicon molecule with the molecular formula SiC$_3$H$_2$ is synthesized via molecular hydrogen elimination. In the
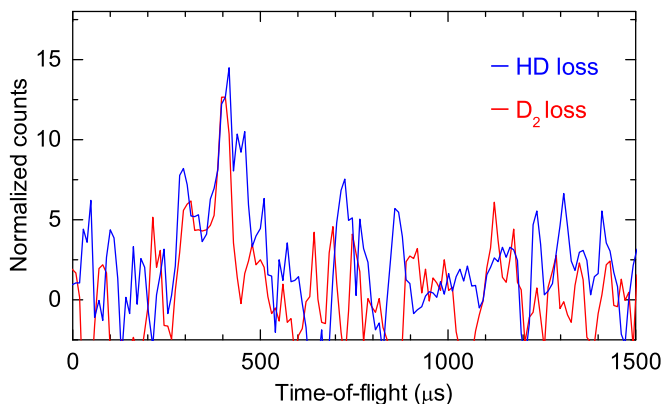

Fig. 2. TOF spectra for the reaction of Si(^{1}D) with D3-methylacetylene (CD$_3$CCH). Recorded at the respective CM angle, the two TOF spectra depict the signal for m/z of 68 (blue line, HD loss) and 67 (red line, D$_2$ loss), corresponding to singly ionized SiC$_3$D$_2$ and SiC$_3$DH molecules, respectively.

case of excited silicon atoms reaction with methylacetylene, the hydrogen atoms are ejected from distinct carbon atoms of the methyl and acetylic group. We attempt now to identify the product isomer(s) formed. This requires an extraction of the underlying reaction dynamics by converting the laboratory data into the CM reference frame. Fig. 3 depicts the CM translational energy distributions $P(E_T)$s and CM angular distributions $T(\theta)$s for the molecular hydrogen loss channel leading to SiC$_3$H$_2$ isomer(s). Both the Si(^{1}D)–allene and Si(^{1}D)–methylacetylene systems could be fit with similar $P(E_T)$s, i.e., 218 ± 28 and 216 ± 26 kJ mol^{-1}, respectively. Therefore, the $P(E_T)$s can extend up to 217 ± 29 kJ mol^{-1} for the Si(^{1}D)–C$_3$H$_4$ systems, which presents the sum of reaction energy plus the collision energy for those products born without internal (ro-vibrational) excitation. By subtracting the collision energy from the high-energy cutoff, the reaction is determined to be exoergic by 187 ± 31 kJ mol^{-1}. Also, the $P(E_T)$s peak away from zero translational energy depicting a broad maximum around 50–80 kJ mol^{-1}; this finding indicates the existence of a tight exit transition state for the decomposition of the SiC$_3$H$_4$ complex(es) and a significant electron density rearrangement upon molecular hydrogen loss (30). Finally, the $T(\theta)$s are similar in both systems and provide additional information on the reaction dynamics. The $T(\theta)$s cover the complete angular range from 0° to 180° with a nearly forward–backward symmetry. This suggests that the reaction involves indirect scattering dynamics via long-lived SiC$_3$H$_4$ intermediates whose lifetimes are longer than or at least competitive with their rotation periods (31). Also, the distribution maxima around 90° ("sideways" scattering) are clearly visible; this feature proposes geometrical constraints with the molecular hydrogen leaving parallel to the total angular momentum vector and almost perpendicularly to the rotational plane of the decomposing SiC$_3$H$_4$ intermediate(s) (31).

Electronic Structure Calculations—Bimolecular Reactions.
Molecular hydrogen loss channel. Having identified SiC$_3$H$_2$ isomers as the product of the bimolecular gas phase reaction of electronically excited silicon atoms (Si(^{1}D)) with allene and methylacetylene under single collision conditions, we next combine these findings with the computational results to untangle the underlying chemical dynamics and reaction mechanism(s). Reactants, products, intermediates, and transition state structures relevant to the reaction of electronically excited atomic silicon with methylacetylene, allene and D3-methylacetylene have been characterized in the *SI Appendix*, Tables S1–S3. A summary of these results is shown in Fig. 4, in the form of zero-point corrected energies, which are slightly simplified by eliminating all transition states that are above the experimental collision energy of 30 ± 2 kJ mol^{-1} and hence cannot be overcome (see *SI Appendix*, Fig. S2 for a full version of the surface). For both reaction systems, the formation of isomers **p1**–**p4** correlates well with the experimentally determined reaction exoergicity of 187 ± 31 kJ mol^{-1} (Fig. 4).

In detail, the computations predict that both reactions are initiated by a barrierless addition of the Si(^{1}D) atom to the π electron density of the hydrocarbon reactant. For methylacetylene, Si(^{1}D) adds to the carbon–carbon triple bond, yielding intermediate [i1], which is the most stable of the SiC$_3$H$_4$ isomers. From [i1], the system can isomerize to [i2], [i4], [i5], and [i6] with barriers of 305, 188, 239, and 256 kJ mol^{-1}, respectively. Despite the lower barrier to [i4], rapid unimolecular decomposition to **p2** via [i4] → [i13] → **p2** is stifled by a barrier of 260 kJ mol^{-1} for the two-step process. Isomer [i5] can readily isomerize to [i2] with a barrier of 19 kJ mol^{-1} or to [i9] with a barrier of 99 kJ mol^{-1}. From [i6], there is very facile isomerization to [i9] and [i12], with barriers of 42 and 60 kJ mol^{-1}, respectively, and also access to [i10] through a barrier of 143 kJ mol^{-1}. Most of the intermediates are thereby capable of interconverting, if products are not too rapidly formed.
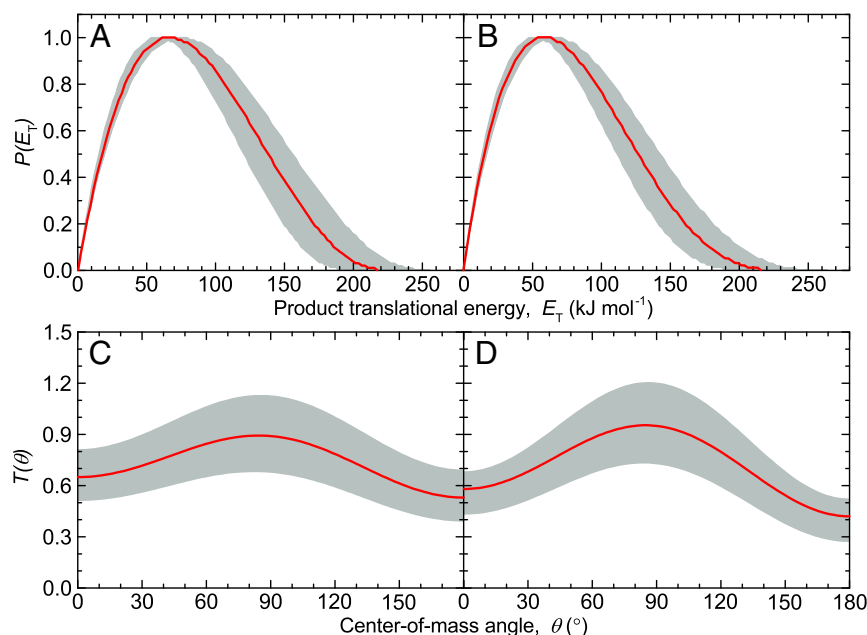
Fig. 3. CM translational energy distributions $P(E_T)$s and CM angular distributions $T(\theta)$s. *A* and *B* are responsible for $P(E_T)$s; *C* and *D* depict $T(\theta)$s, in the reactions of Si(^{1}D) with allene (*A* and *C*) and with methylacetylene (*B* and *D*), leading to the products of SiC_3H_2 isomers and molecular hydrogen. The shaded areas represent the acceptable fits accounting for the 1σ error limits of the laboratory distributions.

Qualitatively this is confirmed by examining the exit barriers for molecular hydrogen loss to form SiC_3H_2. The most favorable exit transition states are the [i6] → **p4** transition state at −114 kJ mol^{-1}, i.e., a barrier of 188 kJ mol^{-1}, the [i9] → **p1** transition state at −89 kJ mol^{-1} with a barrier of 190 kJ mol^{-1}, and two [i12] → **p3** transition states at −71 and −76 kJ mol^{-1} with barriers of 177 and 172 kJ mol^{-1}, but from a high energy intermediate. Exit transition states to **p2** are much higher in energy, with energies of 7, −46, and −46 kJ mol^{-1} for the [i1] → **p2**, [i6]→**p2**, and [i13] → **p2** transition states, respectively. Detailed prediction of branching ratios requires solving the coupled kinetic equations for all of these pathways, after applying

Rice–Ramsperger–Kassel–Marcus (RRKM) theory to obtain the individual rate constants (*SI Appendix*). The outcome for this network is a predicted product distribution of 38.2% **p1**, 0.6% **p2**, 11.1% **p3**, and 45.8% **p4**. The experimental results from the silicon–D3-methylacetylene system, which reveal a branching ratio of 60 ± 15% HD loss and 40 ± 15% D_2 loss, allows for validation of our computed reaction network. Comparing the moderate exit barriers to the comparatively much smaller barriers to isomerization, we expect significant isomerization. Including all possible constitutional isomers in our reaction network, our RRKM calculations predict a product distribution of 56.8% HD loss and
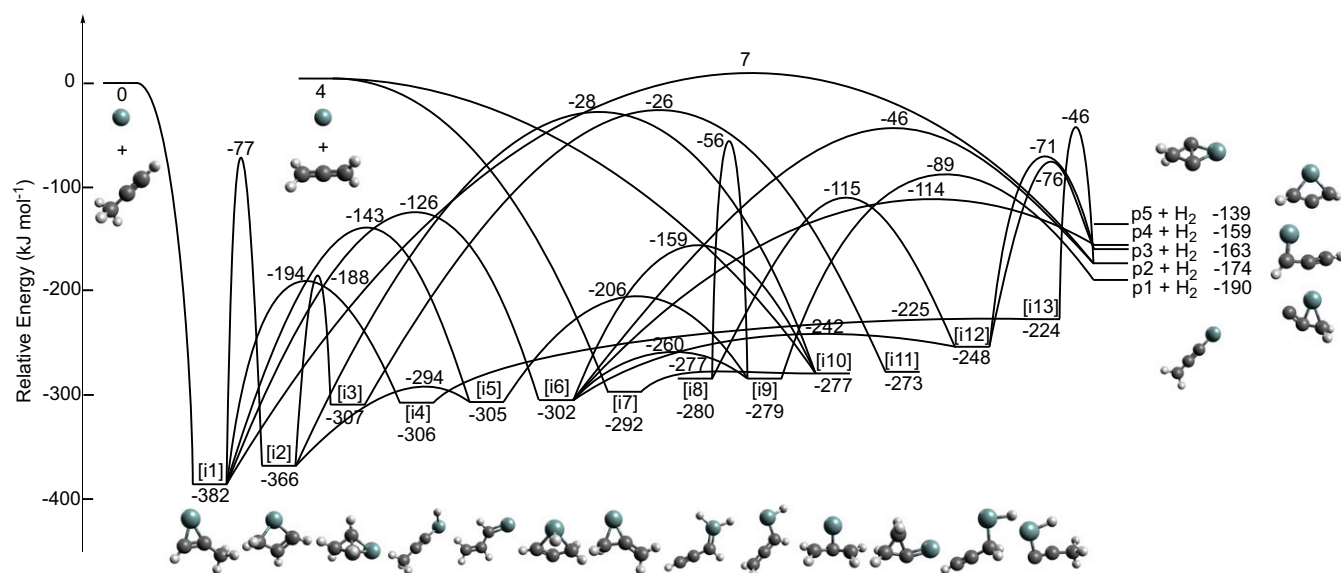

Fig. 4. Pruned potential energy surface for the reactions of Si(^{1}D) with allene and methylacetylene. Relative energies are given in units of kilojoules per mole. The potential energy surface is pruned by removing barriers above the 30 kJ mol^{-1} collision energy (refer to *SI Appendix*, Fig. S2 for the full version). Colors of the atoms: silicon (green), carbon (black), and hydrogen (light gray).

43.2% D_2 loss (*SI Appendix*). This result is in good agreement with experiment, and suggests that the energy landscape shown in Fig. 4 is faithfully capturing the critical aspects of the experimental dynamics observed for Si(^{1}D) with methylacetylene.

Turning next to the computational results for the reaction of Si(^{1}D) with allene, it is evident from Fig. 4 that the silicon atom can add barrierlessly to a C=C bond, yielding a 3-membered ring structure, [i7], or attack the central carbon atom to form the ring-opened isomer [i10]. There is virtually no barrier to ring-opening [i7] to yield [i10]. Intermediate [i10] provides access to the main intermediates already seen in silicon–methylacetylene system. For instance, the sequences [i10] → [i2] → [i1] and [i10] → [i6] → [i1] both access intermediate [i1], the initial encounter product for Si(^{1}D) + methylacetylene. Therefore, the initial collision complexes of the silicon–methylacetylene ([i1]) and silicon–allene ([i7]/[i10]) surfaces are effectively coupled via intermediates [i2] and [i6] with reaction pathways eventually leading to **p1**–**p4** via H_2 loss involving tight exit transition states located 45–167 kJ mol^{-1} above the energy of the separated products. The predicted product distribution for silicon–allene system is therefore very similar to that discussed above for the silicon–methylacetylene system: 38.7% **p1**, 0.5% **p2**, 11.3% **p3**, and 46.5% **p4**.

Atomic hydrogen and methyl loss channels. Having established that the molecular hydrogen loss channel leads predominantly to the formation of the 1-sila-1,2,3-butatrienylidene molecule (H_2C=C=C=Si; X^1A_1; **p1**) and the less stable 4-membered ring structure (c-SiCH=C=CH; **p4**), we also investigated computationally the possibility of atomic hydrogen (H) and methyl (CH_3) loss channels; recall that these channels were not detected experimentally. For the atomic hydrogen loss channel, we located 22 SiC_3H_3 isomers (*SI Appendix*, Table S4). Six isomers—one acyclic (**n1**) and five cyclic molecules (**n2**–**n6**)—are energetically accessible under our experimental conditions at collision energies of 30 ± 2 kJ mol^{-1} holding overall reaction energies from −10 to 24 kJ mol^{-1}. For the methyl loss channels, four SiC_2H isomers could be identified (*SI Appendix*, Table S5), two of which were permitted under experimental conditions with overall reaction energies of −30 and −5 kJ mol^{-1} for **m1** and **m2**, respectively. Statistical (RRKM) calculations were conducted to examine the branching ratios for the energetically accessible hydrogen atom and methyl loss channels (*SI Appendix*, Table S9) versus molecular hydrogen loss. These radical product channels

were found to contribute only about 4% in total to the overall product stream for the silicon–methylacetylene system, and only about 3% of the product stream for the silicon–allene system. These results bolster our experimental findings that the molecular hydrogen loss is the primary dissociation channel and also support the experimental nondetection of atomic hydrogen and methyl group loss channels.

Electronic Structure Calculations—Photodissociation of SiC_3H_2 to Yield SiC_3. We have so far concluded that the bimolecular reactions of electronically excited atomic silicon with allene and methylacetylene lead primarily to the formation of 1-sila-1,2,3-butatrienylidene (H_2C=C=C=Si; X^1A_1) (**p1**) and other SiC_3H_2 isomers (particularly the 4-membered ring, **p4**) under experimental conditions mimicking the conditions in the inner envelope of carbon stars. Ejected by the stellar wind to the outer envelope, the SiC_3H_2 isomers may be dehydrogenated subsequently via photodissociation to silicon tricarbide isomers (SiC_3) such as to the astronomically observed silicon tricarbide (c-SiC_3) by, e.g., interstellar Lyman-α photons (10.2 eV or 984 kJ mol^{-1} for hydrogen). Our computations on the interconversion and molecular hydrogen loss pathways of SiC_3H_2 isomers are summarized in Fig. 5 (see also *SI Appendix*, Table S6). From Fig. 5, it is evident that H_2C=C=C=Si (**p1**) can readily isomerize via ring closure to **p2**; likewise c-SiCH=C=CH (**p4**) can readily isomerize to **p3**.

Considering that the total system energy under experimental conditions is 220 kJ mol^{-1} above **p1**, it is clear that molecular hydrogen loss and other isomer interchange pathways such as **p1** ↔ **p3** are closed unless the SiC_3H_2 isomers are further activated. This is most likely to occur by absorbing Lyman-α photons from the interstellar radiation field. As shown in the *SI Appendix*, Table S7, all five product isomers have excited states that carry significant oscillator strength in the region of 10.2 eV, with the strongest absorbers being **p2** (10.2 eV, f = 0.20) and **p4** (10.2 eV, f = 0.25). Upon photon absorption and rapid nonradiative relaxation to an extremely vibrationally hot electronic ground state, this very large excess internal energy is sufficient to interconvert all SiC_3H_2 isomers and to readily surmount the barriers to molecular hydrogen loss, leading to formation of three SiC_3 isomers [1], [2], and [3], as shown in Fig. 5.

In agreement with our results, previous calculations revealed that c-SiC_3(X^1A_1) [1] represents the thermodynamically most
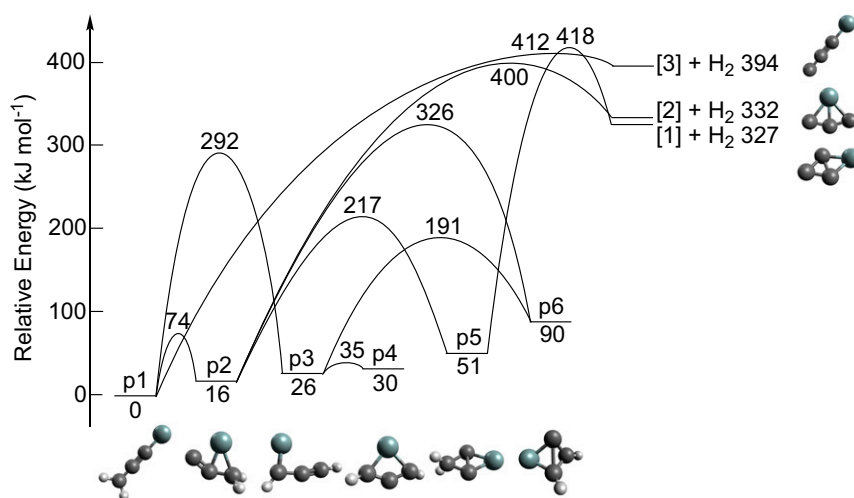

Fig. 5. Potential energy surface for interconversion of SiC_3H_2 isomers and H_2 elimination to yield SiC_3. Relative energies are given in units of kilojoules per mole; the zero of energy is taken as the ZPE-corrected energy of H_2C=C=C=Si The total internal energy of the system under experimental conditions is 220 kJ mol^{-1}. Colors of the atoms: silicon (green), carbon (black), and hydrogen (light gray).

stable silicon tricarbide isomer comparing with c-SiC$_3$(X^{1}A$_1$) [2], which has a transannular silicon–carbon bond, being 8–52 kJ mol^{-1} less stable than [1] (32–39). A second linear isomer (CSiCC) has been predicted to be about 318 kJ mol^{-1} higher in energy compared with (l-SiC$_3$; X^{3}Σ$^-$) (40). The rhomboidal C$_{2v}$ symmetric isomer c-SiC$_3$ (X^{1}A$_1$) [1] that contains a transannular carbon–carbon bond (41, 42), has been observed in the circumstellar envelope of IRC +10216. We also computationally investigated alternative photodissociation pathways from **p1**, **p2**, and **p5** via atomic hydrogen loss (*SI Appendix,* Table S8). These channels are endoergic between 387 and 410 kJ mol^{-1}. While these reaction energies are close to the transition state energies for the molecular hydrogen loss, the molecular hydrogen loss channels are thermodynamically preferred and would be enhanced via tunneling, leading us to suggest that molecular hydrogen loss is the main photodissociation pathway and will produce c-SiC$_3$ (X^{1}A$_1$) [1].

Astrochemical Modeling. Having established that the cyclic silicon tricarbide molecule (c-SiC$_3$) can be formed via photodissociation of 1-sila-1,2,3-butatrienylidene (SiC$_3$H$_2$; H$_2$C=C=C=Si; X^{1}A$_1$), which is generated via bimolecular reactions of electronically excited atomic silicon atom with allene and methylacetylene, we explore how our findings transfer to the circumstellar envelope of IRC+10216 through astrochemical modeling. This is central since crossed molecular beam experiments along with computations cannot adequately simulate conditions in circumstellar environments, such as in the presence of multiple reactants and where the photodissociation of newly formed molecules plays a fundamental role (17). We performed simulations using a network of gas phase reactions in the circumstellar envelope of the carbon rich star IRC+10216 via the chemical kinetic data of the RATE12 release from the UMIST Database for Astrochemistry (17). Physical parameters for the simulations of the inner to outer envelopes were adopted from Li et al. (43). This reaction network was updated by the additional reactive and photodissociation chemistries of the SiC$_3$H$_2$ molecule as elucidated in the present work with initial fractional abundances of the reactive species relative to molecular hydrogen taken from the models of refs. 17 and 43.

These modeling studies lead to fascinating conclusions. First, the astrochemical modeling reveals multiple sources of electronically excited silicon atoms in the inner envelope: photodissociation of silane (SiH$_4$) (44) and (photo)fragmentation of two silicon-bearing diatomic molecules silicon monoxide (SiO) and silicon monosulfide (SiS), which in turn can be generated from shock-induced sputtering of silicon-bearing grains in the inner envelope of the carbon star (19, 45). Silane, silicon monoxide, and silicon monosulfide were detected in the circumstellar envelope at fractional abundances of 2.2×10^{-7}, 1.8×10^{-7}, and 1.3×10^{-6} with respect to molecular hydrogen (17, 43). Note that Suto and Lee examined the photodissociation of silane in the range of 106–160 nm, revealing that electronically excited silicon atoms contribute up to 1.2% of the photodissociation yield (44). Based on that, the overall silicon budget reaches peak fractional abundance above 1.0×10^{-6}, and electronically excited silicon atoms might constitute up to 1% due to photodissociation. Second, the coupling of the silicon with the carbon chemistries leads to present-day fractional abundances of allene (H$_2$CCCH$_2$), methylacetylene (CH$_3$CCH) (46), and silicon tricarbide (c-SiC$_3$) between 7.0×10^{-9} and 8.0×10^{-9} at a radius of about 4×10^{16} cm, while silicon tetracarbide (SiC$_4$) shows a much lower peak abundance of 2.0×10^{-10} (Fig. 6).

The modeling suggests that our proposed mechanism can contribute up to an 80% increase in the column density of the total silicon tricarbide budget. Our channels constitute an experimentally and computationally validated reaction mechanism based on neutral–neutral reactions followed by photo processing, which complements previously proposed networks of ion–molecule reactions
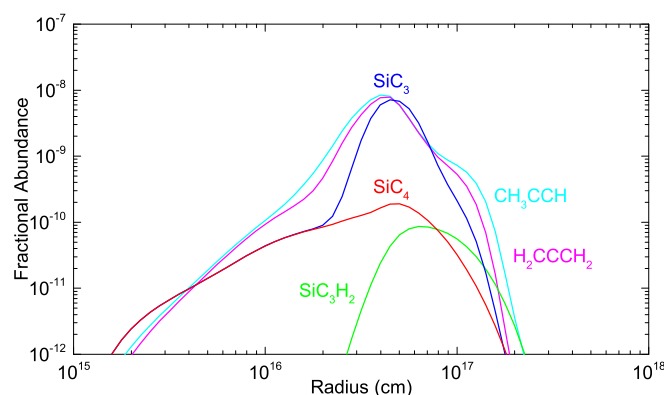

Fig. 6. Modeled present-day fractional abundances of key species related to the formation of silicon tricarbide (c-SiC$_3$) relative to molecular hydrogen. The relative fractional abundances of allene (H$_2$CCCH$_2$), methylacetylene (CH$_3$CCH), 1-sila-1,2,3-butatrienylidene (SiC$_3$H$_2$), silicon tricarbide (SiC$_3$), and silicon tetracarbide (SiC$_4$) are plotted as a function of radius for the circumstellar envelope of the carbon star IRC +10216.

that are less well characterized (*SI Appendix*). It should be highlighted that the fractional abundance of silicon tricarbide (c-SiC$_3$) likely represents a lower limit since only Lyman-α photons were considered in our model to photodissociate SiC$_3$H$_2$ (*SI Appendix,* Table S7). Further, the modeled fractional abundances of SiC$_3$ and of SiC$_4$ clearly indicate that SiC$_4$ cannot represent a precursor of SiC$_3$. Note that in an early study, Apponi et al. commented that SiC$_3$ and SiC$_4$ held column densities of 4.3×10^{12} and 2.7×10^{12} cm^{-2} assuming that both have the same 40"-diameter shell as silicon dicarbide (SiC$_2$); however, up-to-date models predict that 20"- and 25"-diameter shells have to be considered for SiC$_3$ and SiC$_4$, respectively (17, 43), thus suggesting that conclusions drawn from older models have to be adjusted.

Finally, it is important to note that fractional abundances of SiC$_3$H$_2$ of about 10^{-10} are still predicted to be present today and are hence observable in prospective searches in the circumstellar shell. Therefore, the astrochemical modeling reveals the potential for bimolecular reactions of electronically excited silicon atoms (Si(^{1}D)) with allene (H$_2$CCCH$_2$) and methylacetylene (CH$_3$CCH) to initiate the formation of SiC$_3$H$_2$ molecules in the inner envelope. Then, driven by the stellar wind to the outer envelope, subsequent photodissociation of the SiC$_3$H$_2$ parent is efficient in the formation of the bicyclic silicon tricarbide (c-SiC$_3$) daughter species via dehydrogenation.

Conclusions

On the bimolecular reactions of electronically excited silicon atoms (Si(^{1}D)) with allene and methylacetylene, our combined experimental and computational investigation unraveled indirect scattering dynamics initiated through the barrierless addition of silicon to the π electronic systems of the hydrocarbon reactants leading to distinct SiC$_3$H$_4$ collision complexes. These intermediates are formed with internal energy, enabling them to interconvert and ultimately undergo unimolecular decomposition by molecular hydrogen loss to form at least 1-sila-1,2,3-butatrienylidene (H$_2$C=C=C=Si; X^{1}A$_1$) (**p1**) among other isomers. The product isomer distribution is then predicted by a kinetic network developed computationally that is validated by excellent agreement with the H$_2$/HD ratio observed experimentally for the silicon–D3-methylacetylene system. The experiment was conducted at a collision energy of 30 ± 2 kJ mol^{-1}, which is equivalent to a temperature of about 3,500 K that is comparable to conditions in circumstellar envelopes of carbon-rich stars reached by pulsations and inherent shocks in the ejected stellar material (19). The newly formed 1-sila-1,2,3-butatrienylidene (SiC$_3$H$_2$) formed in the inner

Yang et al.

envelope via reaction **I**, can then be transported by the stellar wind to the thinner, outer envelope. In these regions, as demonstrated computationally and via astrochemical modeling, the interstellar UV field can photolyze 1-sila-1,2,3-butatrienylidene (SiC_3H_2) to the bicyclic silicon tricarbide isomer c-$SiC_3(X^1A_1)$ **[1]** as observed in the envelope of IRC+10216 via dehydrogenation (reaction **II**).

This system illustrates the concept of an excited-state-induced synthesis of exotic organosilicon molecules (SiC_3H_2) in the inner circumstellar envelope via the reaction of electronically excited silicon atoms with ubiquitous hydrocarbons, with the parent species undergoing photochemical processing in the outer envelope to cyclic silicon tricarbide (c-SiC_3). Previous models proposed that silicon tricarbide is formed by photodissociation of silicon tetracarbide (SiC_4) (4, 15, 47), but the predicted column density of SiC_4 is two orders of magnitude less than those being observed astronomically in the circumstellar envelope of IRC+10216 (17, 43). Therefore, although some c-$SiC_3(X^1A_1)$ may originate from photodissociation of $SiC_4(X^1A_1)$, the computations along with astrochemical models study identify hydrogenated silicon-carbon species—the isomers of SiC_3H_2—as a key source of c-$SiC_3(X^1A_1)$. (Note that the 1-sila-1,2,3-butatrienylidene parent has not been searched for in the circumstellar envelope of IRC+10216 yet.) This facile route to silicon tricarbide via a single, bimolecular neutral–neutral reaction to a hydrogenated parent molecule followed by photochemical dehydrogenation to a bare silicon–carbon molecule represents a shift away from currently accepted views. It provides an explanation for the previously elusive origin of circumstellar organosilicon molecules eventually constraining the level of molecular complexity, which can be expected in carbon-rich, circumstellar environments. Although the interstellar photon field is more complex than considered in our photodissociation study, which was restricted to Lyman-α, this proof-of-concept study opens up a hitherto overlooked possibility of distinct chemistries in the inner and outer circumstellar envelop of IRC+10216 eventually leading to silicon tricarbide c-$SiC_3(X^1A_1)$. This result challenges the conventional wisdom that circumstellar silicon carbide molecules can only be formed at elevated temperatures via complex ion–molecule reactions or photodegradation of higher molecular weight silicon carbon molecules. With the commission of the Atacama Large Millimeter/Submillimeter Array, the detection of unusual silicon-bearing molecules will continue to grow, and an understanding of these data will rely on advances in experimental and computational laboratory astrophysics as proposed here, thus eliminating the gap between observational and laboratory data on the circumstellar organosilicon chemistry that has existed for decades.

Materials and Methods

Experimental. We carried out the crossed molecular beam reactions of ground and excited state silicon atoms ($Si(^3P)/Si(^1D)$) with allene (H_2CCCH_2; X^1A_1) and methylacetylene (CH_3CCH; X^1A_1) utilizing a universal crossed molecular beam machine (29, 48–50). A pulsed supersonic beam, which contains silicon atoms ($Si(^3P)/Si(^1D)$) and silylidyne radicals ($SiH(X^2\Pi)$), was prepared via photolysis of 0.5% disilane (Si_2H_6; 99.998%; Voltaix) seeded in helium (He; 99.9999%; Gaspro). This gas mixture was introduced into a pulsed valve operating at a backing pressure of 1,520 Torr in the primary source chamber. To generate the reactive silicon species, the output of an excimer laser (ArF, 193 nm, 30 mJ per pulse; Coherent) was focused with a 1.5-m lens downstream of the pulse valve nozzle to an area of 1×4 mm. The pulsed molecular beam then passed through a skimmer, and a four-slit chopper wheel rotating at 120 Hz chose a section of the beam with a defined peak velocity (v_p) and speed ratio (S) of $1,735 \pm 20$ ms^{-1} and 19 ± 2, respectively. This pulse crossed the most intense sections of pulsed beams of allene (98%; Organic Technologies) and methylacetylene (99%; Organic Technologies) at a backing pressure of 550 Torr perpendicularly in the interaction region. Peak velocities and speed ratios of the hydrocarbons were determined to be 790 ± 10 ms^{-1} and 12 ± 1, for allene and methylacetylene yielding a collision energy of 30 ± 2 kJ mol^{-1} and a CM angle of $33 \pm 1°$. To define the position of the molecular hydrogen loss,

experiments also were conducted with D3-methylacetylene (CD_3CCH; 99 atom % D; CDN Isotopes) at the CM angle for economic reasons.

The neutral products were mass filtered after ionization exploiting a quadrupole mass-spectrometer operated in the TOF mode; the ions were detected by a Daly-type detector located in a rotatable, triply differentially pumped ultrahigh vacuum chamber (1×10^{-11} Torr) after electron-impact ionization of the neutral products. The detector can be rotated within the plane defined by both reactant beams to collect up to 6×10^5 angular-resolved TOF spectra. The TOF spectra were then integrated and normalized to the intensity of the TOF at the CM angle to provide the laboratory angular distribution. To provide meaningful information on the scattering dynamics, the laboratory data were transformed into the CM frame exploiting a forward-convolution routine resulting in an angular flux distribution, $T(\theta)$, and translational energy flux distribution, $P(E_T)$, in the CM system (51–53). For the fitting, we adapted a reactive scattering cross-section of an $E_T^{-1/3}$ energy dependence with E_T defining the translational energy within the line-of-center model for barrierless entrance and exoergic reactions governed by long-range attractive forces (54, 55).

Theoretical. Structures for the reactants, intermediates, and products were obtained via geometry optimizations and frequency calculations using the ωB97X-V (56) density functional and the cc-pVTZ basis set (57). This functional is known to be among the most accurate density functionals for thermochemistry and reaction barrier heights (58). Transition state structures were calculated using the freezing string method (59) to generate an initial structure and Hessian which were then refined by a transition state search using the partitioned-rational function optimization eigenvector following method (60) and followed by a frequency calculation. These calculations were also carried out at the ωB97X-V/cc-pVTZ level of theory. The vibrational analysis was used to confirm that the minima have no imaginary frequencies and the transition states have only one imaginary frequency each, as well as to calculate harmonic zero-point energy corrections for the structures. Density functional theory calculations were all carried out using an ultra-fine integration grid consisting of 99 radial points and 590 angular points. To further improve the accuracy of the results for relative energies and barrier heights, single point energy calculations were performed at the minima and transition states. The objective was to approach the complete basis set (CBS) limit using coupled cluster with single, double, and perturbative triple excitations (CCSD(T)) (61). To this end, CCSD(T)/cc-pVTZ calculations using a frozen core approximation were combined with second-order Møller–Plesset perturbation theory using the resolution of the identity approximation (RI-MP2) (62, 63), in larger basis sets. The working expression used for the energy of a given structure was:

$$E(CCSD(T)/CBS) = E(HF/cc\text{-}pV5Z) + E^{corr}(RI\text{-}MP2/CBS_{3,4,5})$$
$$+ E^{corr}(CCSD(T)/cc\text{-}pVTZ) - E^{corr}(RI\text{-}MP2/cc\text{-}pVTZ)$$
$$+ ZPE(\omega B97X\text{-}V/cc\text{-}pVTZ).$$

$E^{corr}(RI\text{-}MP2/CBS_{3,4,5})$ is the extrapolated RI-MP2 correlation energy using the cc-pVTZ, cc-pVQZ, and cc-pV5Z basis sets to fit

$$E^{corr}(RI\text{-}MP2/cc\text{-}pVNZ) = E^{corr}(RI\text{-}MP2/CBS_{3,4,5}) + AN^{-3},$$

where N denotes the cardinal number for the cc-pVNZ basis sets (64). These CCSD(T)/CBS energies are typically accurate to about 3–4 kJ mol^{-1}. The energy of the silicon atom in the ^1D state was calculated by computing the energy of the atom on its triplet ground state and corrected with an experimentally derived triplet-singlet gap (75.4 kJ mol^{-1}) taken from the National Institute of Standards and Technology Atomic Spectra Database. Time-dependent density functional theory (65) calculations were also carried out on select SiC_3H_2 species to search for electronic excited states corresponding to the absorption of a Lyman-α photon. All calculations were performed using the Q-Chem suite of electronic structure programs (66). For further analysis, the RRKM (67) rate constants for select dehydrogenation pathways of SiC_3H_4 isomers were approximated using a Beyer–Swinehart direct state counting algorithm (68) modified to include vibrational tunneling as suggested by Miller (69).

1. T. J. Millar, C. M. Leung, E. Herbst, How abundant are complex interstellar molecules? *Astron. Astrophys.* **183**, 109–117 (1987).
2. L. A. M. Nejad, T. J. Millar, Chemical modelling of molecular sources. *Astron. Astrophys.* **183**, 279–286 (1987).
3. J. H. Bieging, N.-Q. Rieu, Evidence for ion-molecular chemistry in the envelope of IRC+10216. *Astrophys. J.* **329**, L107–L111 (1988).
4. D. A. Howe, T. J. Millar, The formation of carbon chain molecules in IRC+10216. *Mon. Not. R. Astron. Soc.* **244**, 444–449 (1990).
5. T. J. Millar, E. Herbst, R. P. A. Bettens, Large molecules in the envelope surrounding IRC+10216. *Mon. Not. R. Astron. Soc.* **316**, 195–203 (2000).
6. M. C. McCarthy, C. A. Gottlieb, H. Gupta, P. Thaddeus, Laboratory and astronomical identification of the negative molecular ion C6H⁻. *Astrophys. J.* **652**, L141–L144 (2006).
7. I. Cherchneff, A. E. Glassgold, The formation of carbon chain molecules in IRC+10216. *Astrophys. J.* **419**, L41 (1993).
8. T. J. Millar, E. Herbst, A new chemical model of the circumstellar envelope surrounding IRC+10216. *Astron. Astrophys.* **288**, 561–571 (1994).
9. R. I. Kaiser, D. Stranges, Y. T. Lee, A. G. Suits, Neutral-neutral reactions in the interstellar medium. I. Formation of carbon hydride radicals via reaction of carbon atoms with unsaturated hydrocarbons. *Astrophys. J.* **477**, 982–989 (1997).
10. R. I. Kaiser, Experimental investigation on the formation of carbon-bearing molecules in the interstellar medium via neutral-neutral reactions. *Chem. Rev.* **102**, 1309–1358 (2002).
11. V. Wakelam et al., Reaction networks for interstellar chemical modelling: Improvements and challenges. *Space Sci. Rev.* **156**, 13–72 (2010).
12. D. E. Woon, Ed., *The Astrochymist–Resources for Astrochemists and Interested Bystanders*. http://astrochymist.org/. Accessed June 10, 2019.
13. P. Thaddeus, S. E. Cummins, R. A. Linke, Identification of the SiCC radical toward IRC+10216: The first molecular ring in an astronomical source. *Astrophys. J.* **283**, L45–L48 (1984).
14. A. J. Apponi, M. C. McCarthy, C. A. Gottlieb, P. Thaddeus, Astronomical detection of rhomboidal SiC₃. *Astrophys. J.* **516**, L103–L106 (1999).
15. M. Ohishi et al., Detection of a new circumstellar carbon chain molecule, C₄Si. *Astrophys. J.* **345**, L83–L86 (1989).
16. D. D. S. MacKay, S. B. Charnley, The silicon chemistry of IRC+10°216. *Mon. Not. R. Astron. Soc.* **302**, 793–800 (1999).
17. D. McElroy et al., The UMIST database for astrochemistry 2012. *Astron. Astrophys.* **550**, A36 (2013).
18. K. B. Marvel, No methane here. The HCN puzzle: Searching for CH₃OH and C₂H in oxygen-rich stars. *Astron. J.* **130**, 261–268 (2005).
19. L. M. Ziurys, The chemistry in circumstellar envelopes of evolved stars: Following the origin of the elements to the origin of life. *Proc. Natl. Acad. Sci. U.S.A.* **103**, 12274–12279 (2006).
20. O. Morata, E. Herbst, Time-dependent models of dense PDRs with complex molecules. *Mon. Not. R. Astron. Soc.* **390**, 1549–1561 (2008).
21. V. Wakelam et al., A kinetic database for astrochemistry (KIDA). *Astrophys. J. Suppl. Ser.* **199**, 21 (2012).
22. J. Kwan, R. A. Linke, Circumstellar molecular emission of evolved stars and mass loss: IRC+10216. *Astrophys. J.* **254**, 587–593 (1982).
23. M. Agúndez, J. Cernicharo, Oxygen chemistry in the circumstellar envelope of the carbon-rich star IRC+10216. *Astrophys. J.* **650**, 374 (2006).
24. K. Willacy, I. Cherchneff, Silicon and sulphur chemistry in the inner wind of IRC+10216. *Astron. Astrophys.* **330**, 676–684 (1998).
25. M. Agúndez et al., Molecular abundances in the inner layers of IRC+10216. *Astron. Astrophys.* **543**, A48 (2012).
26. R. I. Kaiser, S. P. Krishtal, A. M. Mebel, O. Kostko, M. Ahmed, An experimental and theoretical study of the ionization energies of SiC₂Hₓ (x = 0, 1, 2) isomers. *Astrophys. J.* **761**, 178 (2012).
27. T. Yang et al., Combined experimental and theoretical study on the formation of the elusive 2-methyl-1-silacycloprop-2-enylidene molecule under single collision conditions via reactions of the silylidyne radical (SiH; X²Π) with allene (H₂CCCH₂; X¹A₁) and D4-allene (D₂CCCD₂; X¹A₁). *J. Phys. Chem. A* **119**, 12562–12578 (2015).
28. T. Yang, B. B. Dangi, R. I. Kaiser, L. W. Bertels, M. Head-Gordon, A combined experimental and theoretical study on the formation of the 2-methyl-1-silacycloprop-2-enylidene molecule via the crossed beam reactions of the silylidyne radical (SiH; X²Π) with methylacetylene (CH₃CCH; X¹A₁) and D4-methylacetylene (CD₃CCD; X¹A₁). *J. Phys. Chem. A* **120**, 4872–4883 (2016).
29. X. Gu, R. I. Kaiser, Reaction dynamics of phenyl radicals in extreme environments: A crossed molecular beam study. *Acc. Chem. Res.* **42**, 290–302 (2009).
30. R. D. Levine, R. B. Bernstein, *Molecular Reaction Dynamics and Chemical Reactivity* (Oxford University Press, Oxford, U.K., 1987).
31. W. B. Miller, S. A. Safron, D. R. Herschbach, Exchange reactions of alkali atoms with alkali halides: A collision complex mechanism. *Discuss. Faraday Soc.* **44**, 108–122 (1967).
32. M. C. McCarthy, A. J. Apponi, P. Thaddeus, Rhomboidal SiC₃. *J. Chem. Phys.* **110**, 10645–10648 (1999).
33. A. J. Apponi, M. C. McCarthy, C. A. Gottlieb, P. Thaddeus, The rotational spectrum of rhomboidal SiC₃. *J. Chem. Phys.* **111**, 3911–3918 (1999).
34. M. C. McCarthy, A. J. Apponi, C. A. Gottlieb, P. Thaddeus, Laboratory detection of five new linear silicon carbides: SiC₃, SiC₅, SiC₆, SiC₇, and SiC₈. *Astrophys. J.* **538**, 766–772 (2000).
35. G. E. Davico, R. L. Schwartz, W. C. Lineberger, Photoelectron spectroscopy of C₃Si and C₄Si₂ anions. *J. Chem. Phys.* **115**, 1789–1794 (2001).

36. J. F. Stanton, J. Gauss, O. Christiansen, Equilibrium geometries of cyclic SiC₃ isomers. *J. Chem. Phys.* **114**, 2993–2995 (2001).
37. R. Linguerri, P. Rosmus, S. Carter, Anharmonic vibrational levels of the two cyclic isomers of SiC₃. *J. Chem. Phys.* **125**, 34305 (2006).
38. J. M. Rintelman, M. S. Gordon, G. D. Fletcher, J. Ivanic, A systematic multireference perturbation-theory study of the low-lying states of SiC₃. *J. Chem. Phys.* **124**, 034303 (2006).
39. M. J. Maclean, P. C. H. Eichinger, T. Wang, M. Fitzgerald, J. H. Bowie, A theoretical study of the cyclization processes of energized CCCSi and CCCP. *J. Phys. Chem. A* **112**, 12714–12720 (2008).
40. N. Inostroza, M. Hochlaf, M. L. Senent, J. R. Letelier, Ab initio characterization of linear C₃Si isomers. *Astron. Astrophys.* **486**, 1047–1052 (2008).
41. I. L. Alberts, R. S. Grev, H. F. Schaefer, III, Geometrical structures and vibrational frequencies of the energetically low-lying isomers of SiC₃. *J. Chem. Phys.* **93**, 5046–5052 (1990).
42. M. Gomei, R. Kishi, A. Nakajima, S. Iwata, K. Kaya, Ab initio MO studies of neutral and anionic SiCₙ clusters (n= 2-5). *J. Chem. Phys.* **107**, 10051–10061 (1997).
43. X. Li, T. J. Millar, C. Walsh, A. N. Heays, E. F. Van Dishoeck, Photodissociation and chemistry of N₂ in the circumstellar envelope of carbon-rich AGB stars. *Astron. Astrophys.* **568**, A111 (2014).
44. M. Suto, L. C. Lee, Quantitative photoexcitation study of SiH₄ in vacuum ultraviolet. *J. Chem. Phys.* **84**, 1160–1164 (1986).
45. I. Cherchneff, The inner wind of IRC+10216 revisited: New exotic chemistry and diagnostic for dust condensation in carbon stars. *Astron. Astrophys.* **545**, A12 (2012).
46. M. Agúndez, J. P. Fonfría, J. Cernicharo, J. R. Pardo, M. Guélin, Detection of circumstellar CH₂CHCN, CH₂CN, CH₃CCH, and H₂CS. *Astron. Astrophys.* **479**, 493–501 (2008).
47. A. E. Glassgold, G. A. Mamon, *Chemistry and Spectroscopy of Interstellar Molecules* (University of Tokyo Press, Tokyo, Japan, 1992), pp. 261–266.
48. Y. Guo, X. B. Gu, E. Kawamura, R. I. Kaiser, Design of a modular and versatile interlock system for ultrahigh vacuum machines: A crossed molecular beam setup as a case study. *Rev. Sci. Instrum.* **77**, 034701 (2006).
49. X. Gu, Y. Guo, F. Zhang, A. M. Mebel, R. I. Kaiser, Reaction dynamics of carbon-bearing radicals in circumstellar envelopes of carbon stars. *Faraday Discuss.* **133**, 245–275, discussion 347–374, 449–452 (2006).
50. R. I. Kaiser et al., Untangling the chemical evolution of Titan's atmosphere and surface–From homogeneous to heterogeneous chemistry. *Faraday Discuss.* **147**, 429–478, discussion 527–552 (2010).
51. M. F.Vernon, "Molecular-beam scattering," PhD thesis, University of California at Berkeley, Berkeley, CA (1983).
52. P. S. Weiss, "The reaction dynamics of electronically excited alkali atoms with simple molecules," PhD thesis, University of California at Berkeley, Berkeley, CA (1986).
53. R. I. Kaiser et al., A combined crossed molecular beam and ab initio investigation of C₂ and C₃ elementary reactions with unsaturated hydrocarbons–Pathways to hydrogen deficient hydrocarbon radicals in combustion flames. *Faraday Discuss.* **119**, 51–66, discussion 121–143 (2001).
54. R. D. Levine, R. B. Bernstein, Y. T. Lee, Molecular reaction dynamics and chemical reactivity. *Phys. Today* **41**, 90–92 (1988).
55. R. I. Kaiser et al., PAH formation under single collision conditions: Reaction of phenyl radical and 1,3-butadiene to form 1,4-dihydronaphthalene. *J. Phys. Chem. A* **116**, 4248–4258 (2012).
56. N. Mardirossian, M. Head-Gordon, ωB97X-V: A 10-parameter, range-separated hybrid, generalized gradient approximation density functional with nonlocal correlation, designed by a survival-of-the-fittest strategy. *Phys. Chem. Chem. Phys.* **16**, 9904–9924 (2014).
57. R. A. Kendall, T. H. Dunning, Jr, R. J. Harrison, Electron affinities of the first-row atoms revisited. Systematic basis sets and wave functions. *J. Chem. Phys.* **96**, 6796–6806 (1992).
58. N. Mardirossian, M. Head-Gordon, Thirty years of density functional theory in computational chemistry: An overview and extensive assessment of 200 density functionals. *Mol. Phys.* **115**, 2315–2372 (2017).
59. A. Behn, P. M. Zimmerman, A. T. Bell, M. Head-Gordon, Efficient exploration of reaction paths via a freezing string method. *J. Chem. Phys.* **135**, 224108 (2011).
60. J. Baker, An algorithm for the location of transition states. *J. Comput. Chem.* **7**, 385–395 (1986).
61. K. Raghavachari, G. W. Trucks, J. A. Pople, M. Head-Gordon, A fifth-order perturbation comparison of electron correlation theories. *Chem. Phys. Lett.* **157**, 479–483 (1989).
62. M. Feyereisen, G. Fitzgerald, A. Komornicki, Use of approximate integrals in ab initio theory. An application in MP2 energy calculations. *Chem. Phys. Lett.* **208**, 359–363 (1993).
63. D. E. Bernholdt, R. J. Harrison, Large-scale correlated electronic structure calculations: The RI-MP2 method on parallel computers. *Chem. Phys. Lett.* **250**, 477–484 (1996).
64. A. Halkier et al., Basis-set convergence in correlated calculations on Ne, N₂, and H₂O. *Chem. Phys. Lett.* **286**, 243–252 (1998).
65. E. Runge, E. K. U. Gross, Density-functional theory for time-dependent systems. *Phys. Rev. Lett.* **52**, 997–1000 (1984).
66. Y. Shao et al., Advances in molecular quantum chemistry contained in the Q-Chem 4 program package. *Mol. Phys.* **113**, 184–215 (2015).
67. J. I. Steinfeld, J. S. Francisco, W. L. Hase, *Chemical Kinetics and Dynamics* (Oxford University Press, Oxford, U.K., 1990).
68. T. Beyer, D. F. Swinehart, Algorithm 448: Number of multiply-restricted partitions. *Commun. ACM* **16**, 379 (1973).
69. W. H. Miller, Tunneling corrections to unimolecular rate constants, with application to formaldehyde. *J. Am. Chem. Soc.* **101**, 6810–6814 (1979).